Research Square

Preprints are preliminary reports that have not undergone peer review.
They should not be considered conclusive, used to inform clinical practice,
or referenced by the media as validated information.

# Spent Zn–C battery graphite as a direct precursor for graphene oxide and reduced graphene oxide: A reductant-free valorization route

**Gilberto Maia Brito**

gmaiabrito@gmail.com

Federal University of Espirito Santo: Universidade Federal do Espirito Santo https://orcid.org/0000-0001-6205-0511

**Giuliano Martins Santos**

Federal University of Espirito Santo: Universidade Federal do Espirito Santo

**Daniel Fernandes Cipriano**

Federal University of Espirito Santo: Universidade Federal do Espirito Santo

**Miguel Angelo Schettino Jr.**

Federal University of Espirito Santo: Universidade Federal do Espirito Santo

**Jair Carlos Checon Freitas**

Federal University of Espirito Santo: Universidade Federal do Espirito Santo

**Research Article**

**Keywords:**

**Posted Date:** November 25th, 2026

**DOI:** https://doi.org/10.21203/rs.3.rs-11516514/v1

**License:** This work is licensed under a Creative Commons Attribution 4.0 International License.
Read Full License

# *Spent Zn–C battery graphite as a direct precursor for graphene oxide and reduced graphene oxide: A reductant-free valorization route*

Brito, G. M.[1,2], Santos, G. M.[1,2], Cipriano, D. F.[1], Schettino Jr., M. A.[1], Freitas, J. C. C.[1]

[1] Laboratory of Carbon and Ceramics Materials (LMC), Department of Physics - Federal University of Espírito Santo (UFES), Vitória-ES, 29075-910. Brazil.

[2] FAESA University Center, Department of Engineering, Vitória-ES, 29053-360. Brazil.

Corresponding author: gmaiabrito@gmail.com

**Abstract**

The rapid expansion of electronic waste, particularly spent zinc–carbon batteries, poses a mounting environmental burden and calls for circular-economy recovery strategies. Graphite rods from discarded AA Zn–C batteries are an underexploited carbon stream and a potential feedstock for higher-value materials. We propose a simplified route to convert this graphite into graphene-based materials. Recovered graphite was washed with water, dried, sieved and directly oxidised to graphene oxide by a modified Hummers method, without acid leaching or solvent-based purification. Graphene oxide was then converted into reduced graphene oxide by a single thermal treatment (150 °C, 15 h) without chemical reducing agents. Materials were characterised by scanning

electron microscopy, X-ray diffraction, Raman spectroscopy and solid-state $^{13}C$ nuclear magnetic resonance, and benchmarked against graphene oxide from commercial graphite. X-ray results showed interlayer expansion to 0.84 nm for GOW, smaller than for GOC (1.15 nm), and contraction to 0.355 nm after thermal reduction, approaching pristine graphite (0.338 nm). Raman spectra showed a near-invariant $I_D/I_G$ ratio (~0.85) across graphite, GOW, rGOW and GOC ($L_a$ ≈ 22–23 nm), indicating that oxidation mainly disturbs interlayer stacking rather than the in-plane graphitic framework. In $^{13}C$ NMR, the $sp^2$ carbon resonance shifted from 127.9 ppm (GOW) to 126.1 ppm (rGOW), with strongly reduced oxygenated-carbon signals, indicating substantial but partial deoxygenation. Residual zinc sulphate in raw graphite did not prevent oxidation or reduction. These findings show that graphite from spent Zn–C batteries is a viable secondary raw material for graphene-based materials, offering a low-complexity route to electronic-waste valorization.

*Keywords: Waste valorization, Spent Zn–C batteries, Graphite recovery, Graphene oxide, Reduced graphene oxide, Thermal reduction.*

## Graphical Abstract

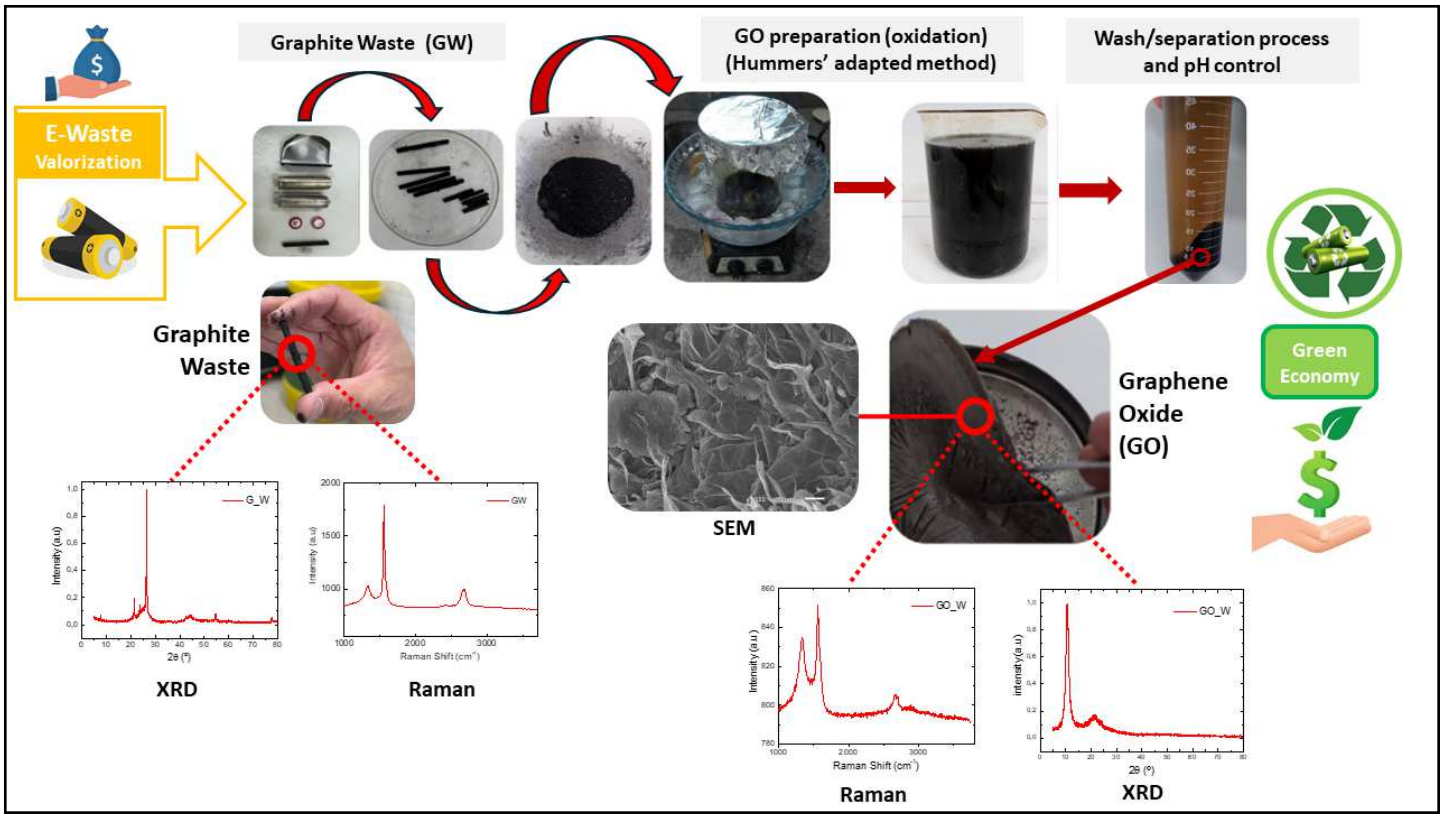

## 1. Introduction

The rapid growth of electronic waste (e-waste), projected to reach 74.7 million metric tons by 2030, has intensified concerns regarding the environmental impact of discarded electrochemical devices (D'Amato et al., 2017). Among these, spent zinc–carbon AA batteries represent a widely available waste stream containing hazardous constituents capable of contaminating soil and water systems. Consequently, strategies focused on material recovery and valorization have gained increasing attention as pathways toward sustainable resource management (Adu et al., 2025; Chakraborty et al., 2022; Houessionon et al., 2021; Ribeiro et al., 2021; Mushahary et al., 2024).

Zinc–carbon batteries contain a central graphite rod that functions as the cathodic current collector. Notably, this graphite rod retains structural integrity after battery depletion and can be mechanically recovered with minimal processing (Rezaei et al., 2025). Such characteristics make graphite from spent AA batteries a promising secondary carbon source for the production of graphene-based materials, particularly graphene oxide (GO) and reduced graphene oxide (rGO) (Adu et al., 2025; Lee et al., 2023) and it has emerged as a viable, cost-effective, and environmentally sustainable raw material (Uppin et al., 2025; Vieira et al., 2023; Ida et al., 2025).

Graphite is a highly ordered hexagonal crystalline mineral composed of stacked graphene layers arranged in a lamellar structure. These layers are held together by weak van der Waals forces and π–π stacking interactions arising from the overlap of delocalized π-electrons within the aromatic rings of adjacent graphene sheets (Singh et al., 2023; Wu et al., 2009).

Graphene is a two-dimensional crystalline carbon material composed of $sp^2$-hybridized atoms arranged in a hexagonal lattice (Singh et al., 2023; Geim et al., 2007). GO is commonly synthesized via oxidative exfoliation of graphite, most frequently using the modified Hummers method (Hummers Jr. et al., 1958; Rawal et al., 2021; Gao et al., 2009).

The oxidation process introduces oxygen-containing functional groups into the graphitic lattice, disrupts π–π stacking interactions, and increases interlayer spacing, facilitating exfoliation into few-layer sheets. Subsequent reduction (thermal or chemical) partially restores the conjugated $sp^2$ carbon network and removes a significant fraction of the oxygen functionalities, yielding rGO with tunable structural disorder and defect density (Vieira et al., 2023; Ida et al., 2025; Sing et al., 2023; Gebreegziabher et al., 2019; Rawal et al., 2021; Gao et al., 2007).

Subsequent thermal or chemical reduction partially restores the conjugated $sp^2$ carbon network, yielding rGO with tunable structural disorder and defect density.

Despite the extensive literature on GO synthesis, most studies rely on high-purity commercial graphite as the precursor material. The feasibility of directly employing graphite recovered from spent AA batteries, without chemical or solvent-based pretreatment, remains insufficiently explored.

Moreover, conventional reduction strategies typically require strong chemical reducing agents, increasing reagent consumption, process complexity, and secondary waste generation. While seminal studies by Dreyer *et al.* and Luo *et al.* established the chemical framework and structural understanding of GO oxidation and reduction mechanisms using commercial graphite, the transferability of these classical protocols to structurally distinct, waste-derived graphite has not been systematically evaluated (Dreyer et al., 2010; Luo et al., 2011).

Therefore, a clear research gap exists in developing simplified and environmentally minimized oxidation–reduction routes using waste-derived graphite as a precursor.

Battery-derived graphite has been explored mainly in the context of spent lithium-ion batteries, where anode graphite is recovered together with metals or converted into GO/rGO for specific applications (Ribeiro et al., 2021; Lee et al., 2023; Uppin et al., 2025; Ida et al., 2025). For spent dry cells, Saha et al. (2025) prepared rGO/$MnO_2$ nanocomposites for supercapacitor electrodes, focusing on composite performance rather than on the structural evolution of the graphene-based materials. To our knowledge, a systematic structural comparison between GO and rGO obtained from spent Zn–C battery graphite and from commercial graphite under identical conditions has not been reported.

Within the broader context of municipal solid waste (MSW) management, spent AA batteries occupy a particularly problematic position: they are generated in enormous volumes by households worldwide, yet their small size and dispersed disposal pattern make them one of the most difficult MSW fractions to capture through formal collection systems. Unlike larger e-waste items that are more readily targeted by take-back schemes, discarded batteries are frequently

disposed of alongside undifferentiated household waste, where their metallic and electrolytic components pose a long-term contamination risk to landfill environments.

From a circular economy perspective, this represents a missed opportunity rather than an unavoidable loss: the graphite rod at the core of each Zn–C battery is a structurally intact, chemically stable carbon reservoir that persists well beyond the electrochemical lifetime of the device. Recovering and re-valorising this component directly addresses two core tenets of circular economy thinking, namely, keeping materials in productive use for as long as possible and designing waste-to-resource pathways that require minimal additional processing.

Framed this way, the conversion of battery-derived graphite into graphene oxide and reduced graphene oxide is not merely a materials-synthesis exercise, but a concrete demonstration of how a routinely discarded MSW fraction can be redirected into a high-value production chain.

In this work, graphite rods recovered from spent zinc–carbon AA batteries were employed directly, following only mild washing, as precursors for GO synthesis

via the modified Hummers method. A subsequent controlled thermal treatment was employed to obtain rGO without the use of chemical reducing agents. In contrast to conventional reduction protocols reported in the literature, the proposed one-step thermal treatment methodology establishes a simplified and environmentally minimized pathway for rGO production (Vieira et al., 2023; Dreyer et al., 2010; Fernández-Merino et al., 2010; Soni et al., 2018; Kondratowicz et al., 2018; Destiarti et al., 2024; Saha et al., 2025; Mulligan-Clarke et al., 2026).

The structural and chemical evolution during oxidation and reduction was systematically investigated by scanning electron microscopy (SEM), X-ray diffraction (XRD), Raman spectroscopy, and nuclear magnetic resonance (NMR) (Vieira et al., 2023; Singh et al., 2023; Luo et al., 2011; Zhu et al., 2024).

By integrating waste-derived graphite with a chemically minimized oxidation–thermal reduction pathway, this study advances a sustainable approach for the production of GO and rGO, reducing reagent demand, limiting hazardous by-products, and expanding the applicability of secondary carbon feedstocks for graphene-based materials.

## 2. Experimental methods

### 2.1 Recovery and preparation of graphite

Spent AA Zn–C batteries of the same type were collected from different locations and manually dismantled in a well-ventilated area, wearing gloves, safety goggles and lab coats, because of the residual electrolyte and metal oxides. After removal of the zinc casing (anode), the graphite rods (cathode current collector) were recovered as waste graphite (GW); all remaining battery components were disposed of as hazardous waste. GW was washed with distilled water under continuous stirring at room temperature to reduce electrolyte salts and discharge by-products adhered to its surface, dried at 60 °C for 5 h and stored in a desiccator. The dried rods were ground manually and sieved (250 mesh) to standardize particle size. Commercial graphite (CG) [supplier, purity and sieving to be stated] was used as reference precursor.

### 2.2 Synthesis of GOW, GOC and rGOW

Graphene oxide from waste graphite (GOW) was prepared through a top-down strategy employing GW as a renewable carbon source, based on the modified Hummers method (Hummers and Offeman, 1958). GW (1.0 g) was dispersed in 70.0 mL of $H_2SO_4$ under constant stirring, and 3.0 g of $KMnO_4$ and 0.5 g of

$NaNO_3$ were added gradually. The mixture was stirred for 2 h in an ice bath to control the exothermic reaction and avoid thermal decomposition of $KMnO_4$. Distilled water (350 mL) was then added and, after 30 min, 10.0 mL of $H_2O_2$ followed by a further 650 mL of water. The suspension stood at room temperature for 72 h, and the supernatant was neutralized and discarded. The product was washed by centrifugation (4000 rpm, 20 min per cycle) until neutral pH and freeze-dried at −50 °C for 72 h (LIOTOP L101). Graphene oxide from commercial graphite (GOC) was prepared by an identical procedure. Reduced graphene oxide (rGOW) was obtained by heating 5.0 g of GOW in a porcelain crucible at 150 °C for 15 h under an oxidizing atmosphere at ambient pressure (101 kPa), and stored in a desiccator. Figure 1 shows schematic structures of graphite, GO (Lerf–Klinowski model; Lerf et al., 1998) and rGO (Singh et al., 2023; Ahmed et al., 2023; Jirickova et al., 2022).

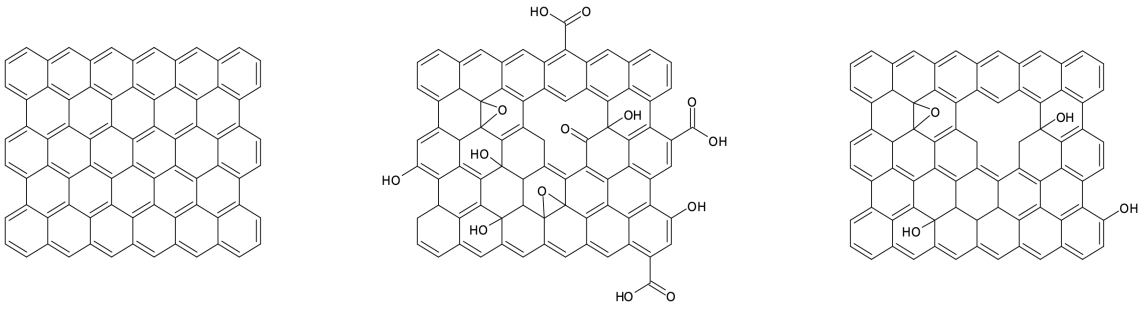


(a) (b) (c)

**Figure 1.** Schematic structural models of (a) graphite, (b) GO, and (c) rGO

### 2.3 Characterization

GW, CG, GOW, GOC and rGOW were characterised by scanning electron microscopy (SEM), X-ray diffraction (XRD), Raman spectroscopy and solid-state $^{13}C$ nuclear magnetic resonance (NMR), following previously reported methodologies (Vieira et al., 2023; Gebreegziabher et al., 2019; Mokoena and Mofokeng, 2024). SEM images were obtained with a JEOL JSM-6610LV microscope at 20 kV, at magnifications of 250× to 10,000×, with powders mounted on aluminium stubs using double-sided carbon tape. XRD patterns were recorded with a Shimadzu XRD-6000 diffractometer (Cu Kα, λ = 1.5418 Å; 40 kV, 30 mA) over 2θ = 5–80° (step 0.02°, 2° $min^{-1}$), with samples packed in a quartz holder. The interlayer spacing (d) and the crystallite size along the c-axis (Lc) were obtained from the (002) reflection using Bragg's law (Eq. 1) and the Scherrer equation (Eq. 2), with n = 1, K = 0.89 and β the full width at half maximum in radians (Cullity and Stock, 2001; Zhou et al., 2014; Iwashita et al., 2004; Vieira et al., 2016; Stobinski et al., 2014). The degree of graphitisation of the graphite samples, G (%), was estimated with Eq. 3, where 0.3440 nm and 0.3354 nm are the interlayer spacings of fully turbostratic carbon and ideal graphite, respectively (Iwashita et al., 2004).

$$d = \frac{n\lambda}{2\sin\theta} \quad (1)$$

$$L_c = \frac{K\lambda}{\beta cos\theta} \quad (2)$$

$$G_{(\%)} = \frac{0.3440 - \mathrm{d}(002)}{0.3440 - 0.3354} \times 100 \quad (3)$$

Raman spectra were acquired with a WITec Alpha300 RA Raman–AFM microscope (532 nm laser, 200 µm confocal aperture, 1 $cm^{-1}$ spectral resolution) at 293 K, with 30 accumulations of 0.5 s per spectrum, and processed with WITec Project FIVE 5.2. The $I_D/I_G$ and $I_{2D}/I_G$ intensity ratios were calculated, and the in-plane crystallite size of the $sp^2$ domains ($L_a$, in nm) was estimated for 532 nm excitation with Eq. 4 (Cançado et al., 2006; Raman, 1928; Bokobza et al., 2015; Yoon et al., 2012).

$$L_a \approx \frac{19.2}{\mathrm{ID/IG}} \quad (4)$$

Solid-state $^{13}C$ NMR spectra were recorded at room temperature on a Varian/ Agilent VNMR 400 MHz spectrometer ($^{13}C$ frequency of 100.52 MHz, 9.4 T) with a triple-resonance probe, using magic-angle spinning at 14 kHz in 4 mm zirconia rotors. Spectra were processed with 200 Hz line broadening and

referenced to tetramethylsilane using hexamethylbenzene (δ = 17.3 ppm) as secondary reference (Freitas et al., 2012; He, 1996).

## 3 Results and discussion

The oxidation of 1.0 g of GW via the modified Hummers method yielded approximately 1.2 g of GOW. The observed mass increase is attributed to the incorporation of oxygen-containing functional groups into the carbon framework during the oxidation process, particularly at the sheet edges.

Comparable mass gains during GO synthesis have been consistently reported in the literature (Dreyer et al., 2010; Marcano et al., 2010). Figure 2 shows a fully disassembled AA Zn–C battery (a) and (b) a single graphite rod recovered prior to the washing process.

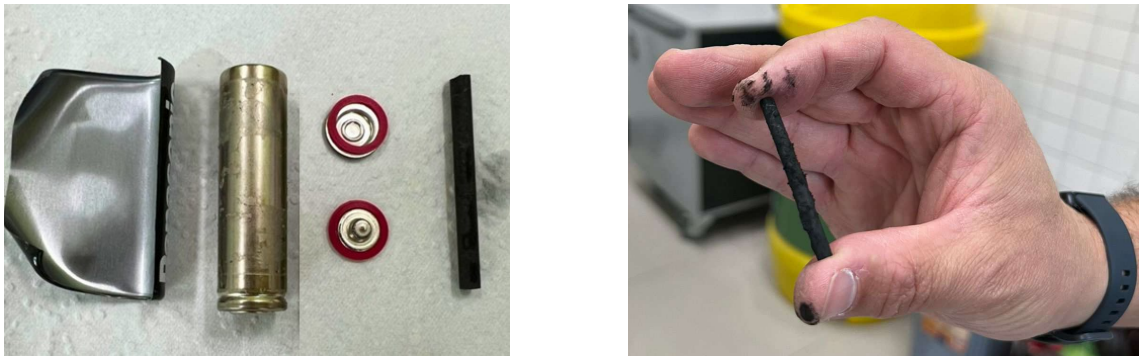

(a) (b)

**Figure 2.** (a) disassembled AA Zn-C battery and (b) a single graphite rod.

Figure 3 shows (a) a flexible GOW sample (approximately 3 mm thick) obtained via the direct oxidation of graphite recovered from AA batteries using a modified Hummers method (Hummers Jr., 1958), and (b) a thin and flexible rGOW film produced through the thermal reduction of the as-prepared GOW.

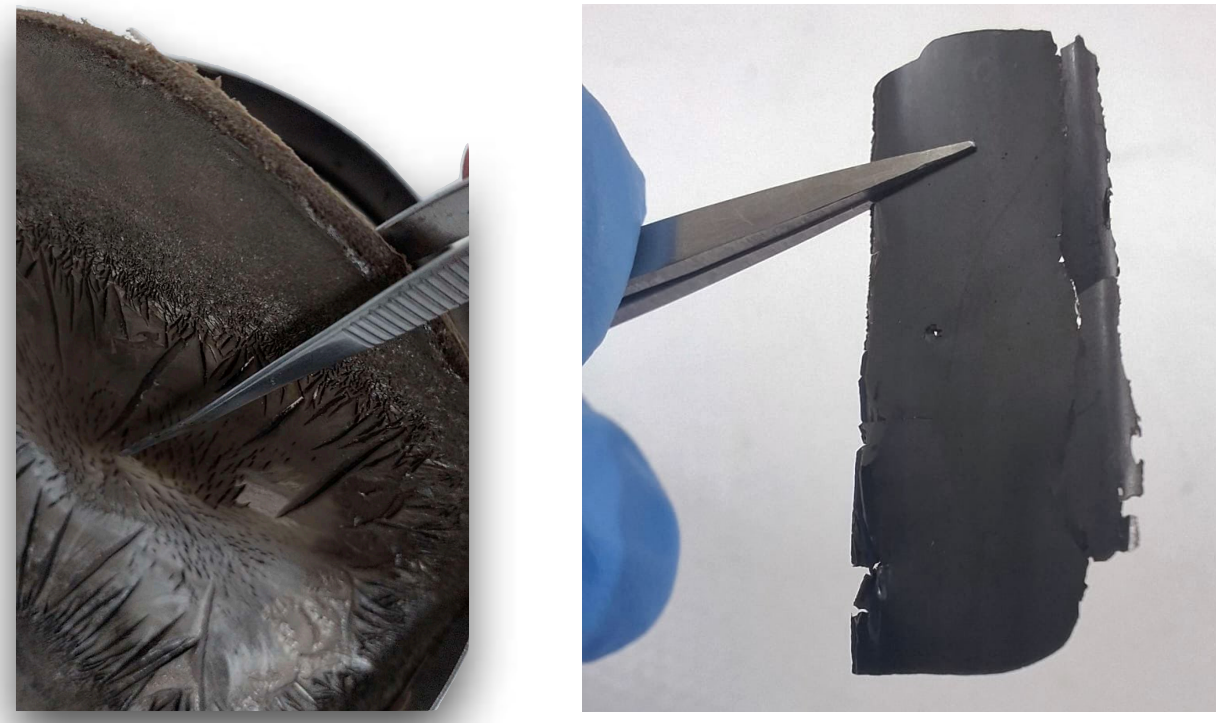

(a) (b)

**Figure 3.** Graphene-based samples: (a) GOW 3 mm thick and (b) thin flexible rGOW.

### 3.1 SEM

Figure 4 presents the SEM micrographs of the analyzed samples. The surface morphology of GW closely resembles that of GC, particularly in terms of particle shape, surface roughness, and texture. Both materials exhibit a characteristic flake-like morphology with smooth, overlapping lamellar layers, indicative of a well-organized crystalline structure associated with stacked graphene planes (Mokoena et al., 2024; Bu et al., 2023).

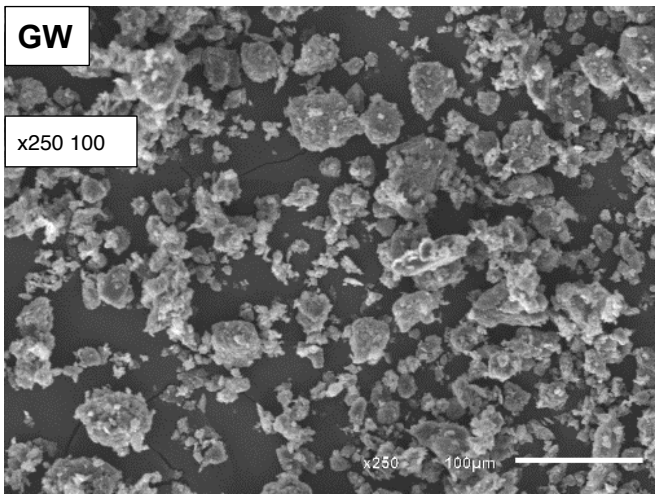


(a)

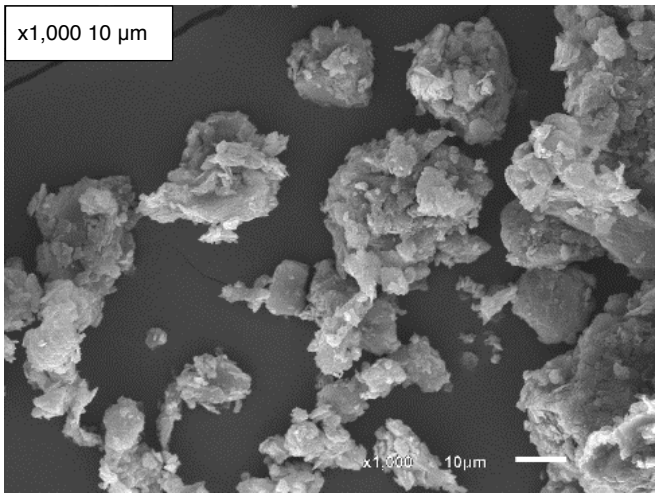

(b)

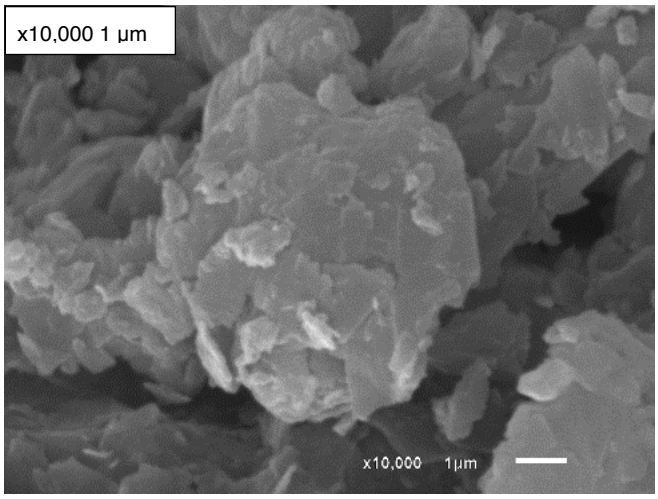


(c)

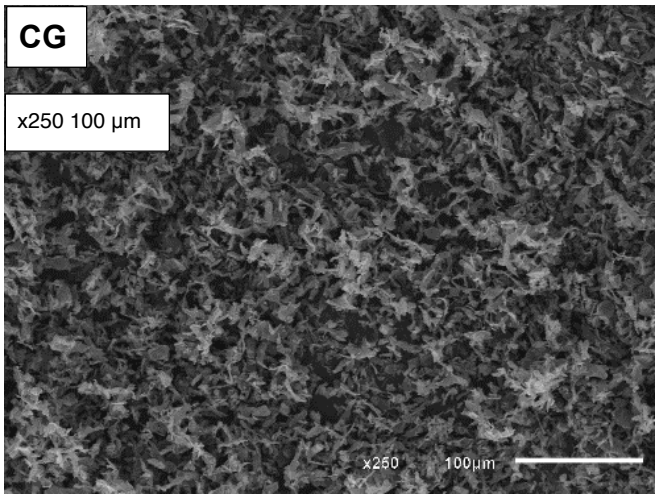


(d)

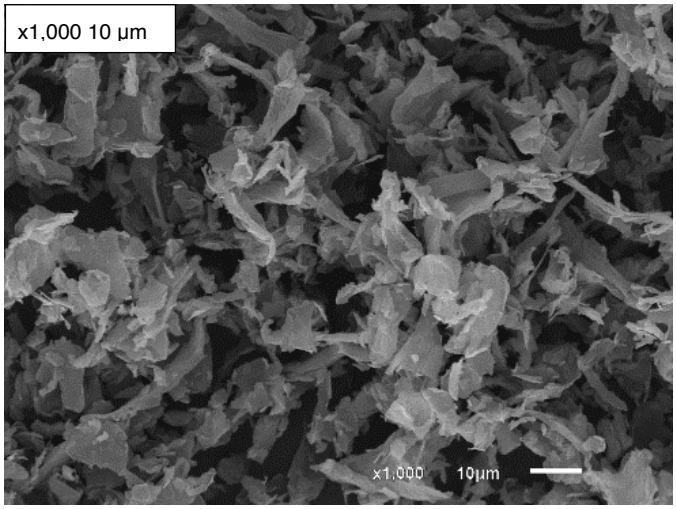


(e)

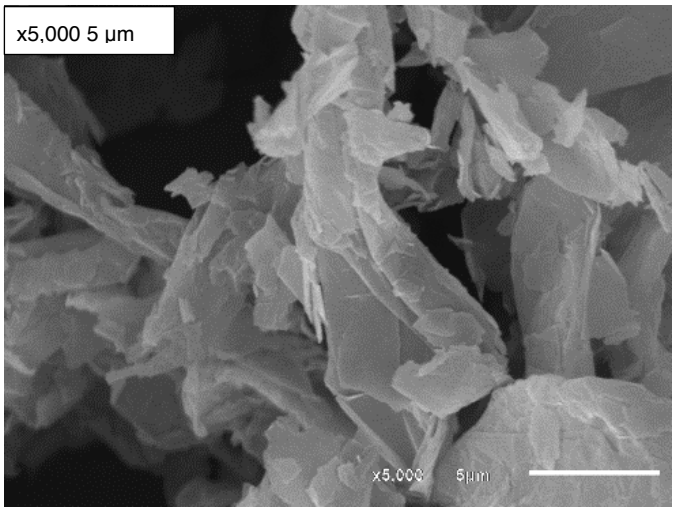


(f)

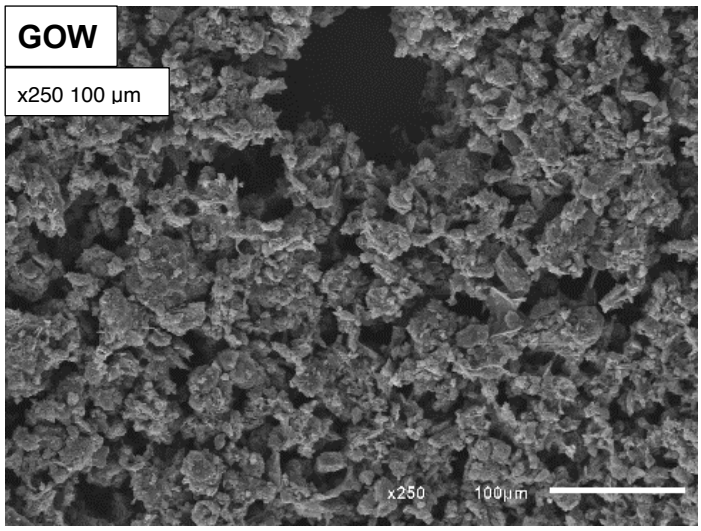
GOW
x250 100 µm
x250
100µm

(g)

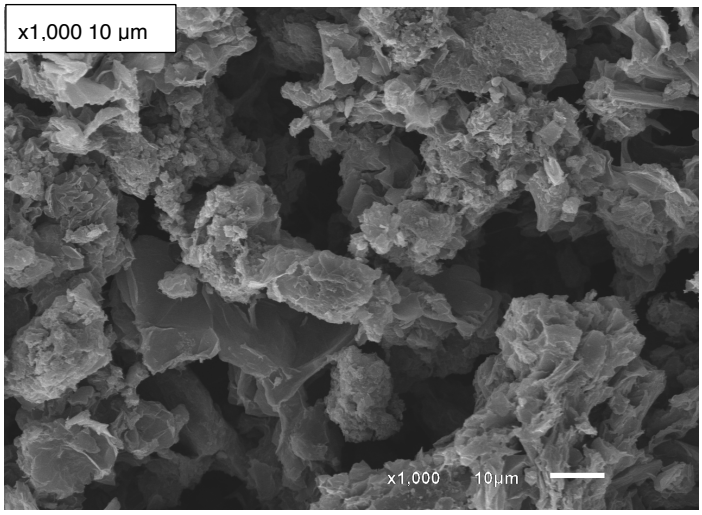
x1,000 10 µm
x1,000
10µm

(h)

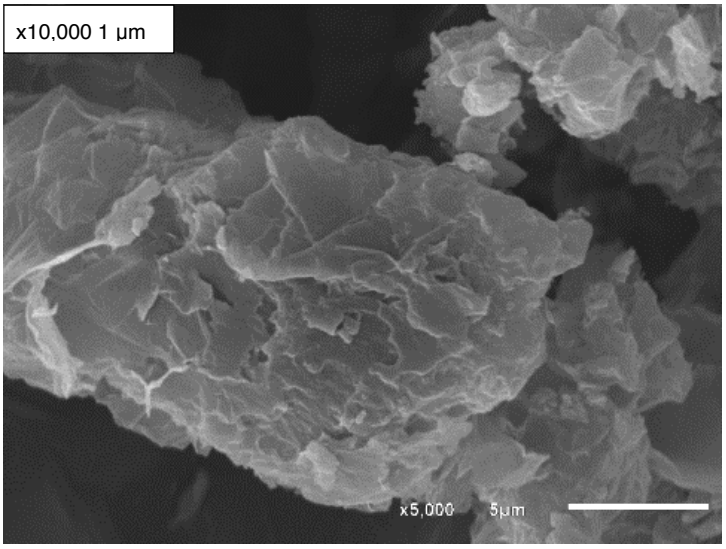
x10,000 1 µm
x5,000
5µm

(i)

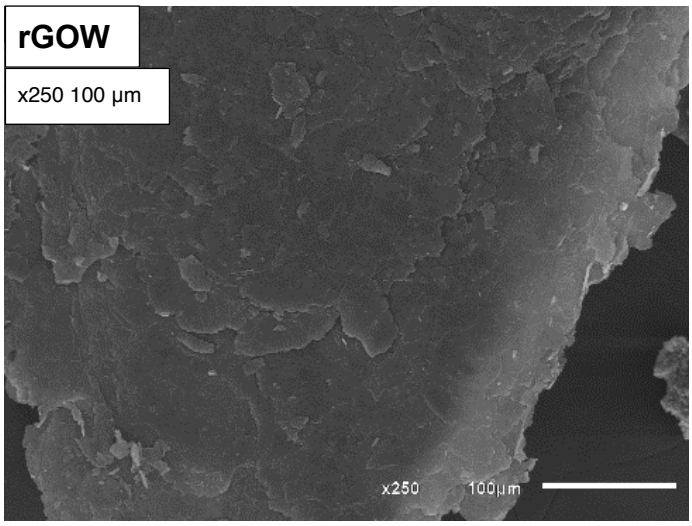


(j)

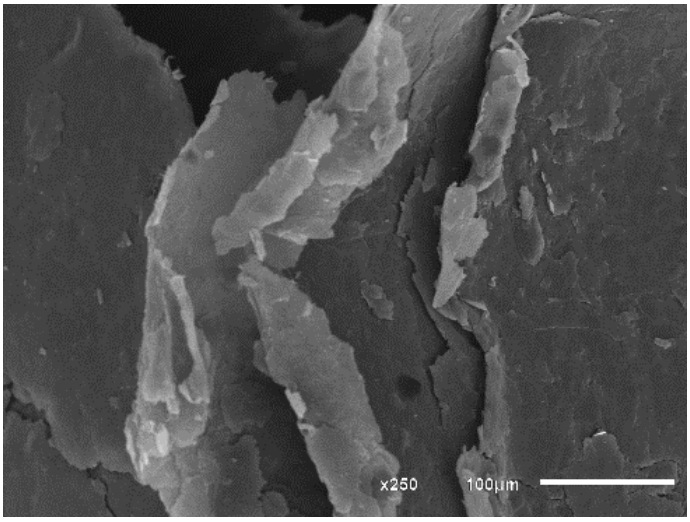


(k)

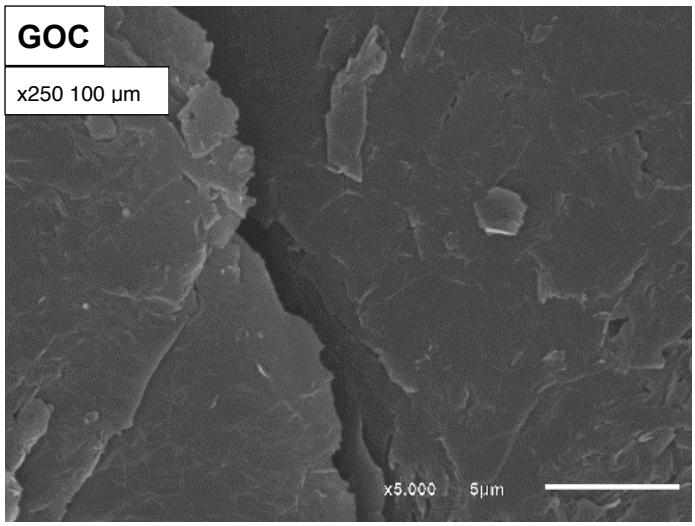


(l)

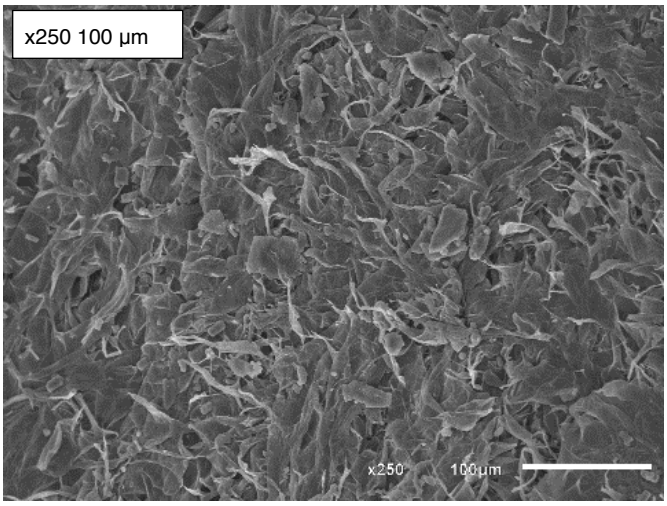


(m)

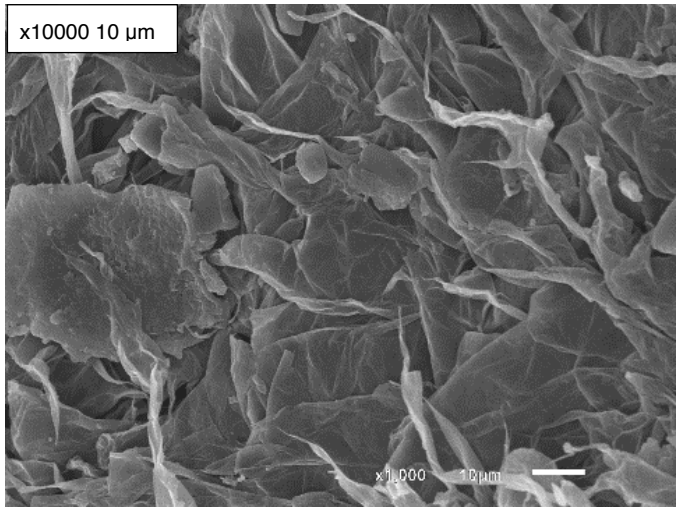


(n)

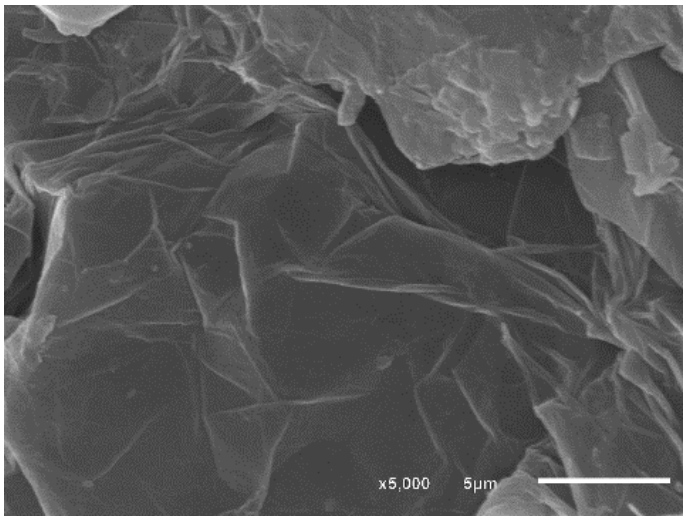


(o)

**Figure 4.** SEM recorded images of the analyzed samples with different magnifications.

Similarly, GOW and GOC display comparable morphological features, characterized by relatively smooth and densely packed sheets, typically formed during the final stages of the oxidation process (Zheng et al., 2012; Mishra et al., 2023). In contrast, the SEM images of rGOW suggest an increased degree of restacking of graphene-based sheets following thermal reduction, leading to the formation of a compact structure (Okhai et al., 2016).

### 3.2 XRD

Figure 5 presents the X-ray diffraction patterns of the graphite- and graphene-based samples. As shown in Figure 5a, a sharp and intense diffraction peak at $2\theta = 26.4°$ (✳) was observed, which is characteristic of the (002) plane of hexagonal crystalline graphite (Gebreegziabher, 2019; Mokoena, 2024; Zhou, 2014; Bu, 2023; Hosseinkhani, 2023).

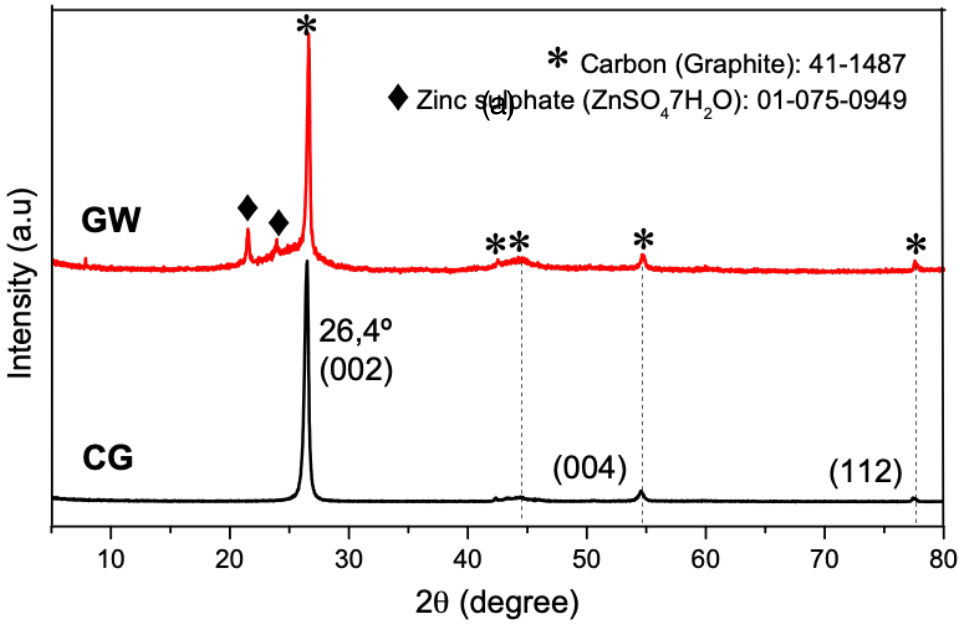
* Carbon (Graphite): 41-1487
♦ Zinc sulphate (ZnSO4 7H2O): 01-075-0949
(a)
GW
CG
26,4º
(002)
(004)
(112)
Intensity (a.u)
2θ (degree)
10
20
30
40
50
60
70
80

(a)

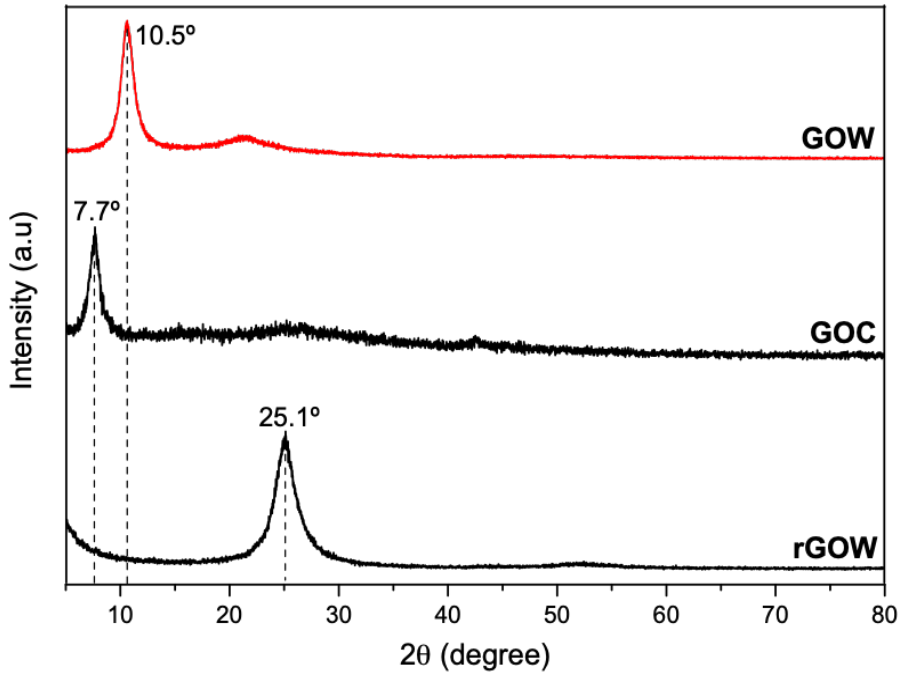
10.5º
GOW
7.7º
GOC
25.1º
rGOW
Intensity (a.u)
2θ (degree)
10
20
30
40
50
60
70
80

(b)

**Figure 5.** XRD pattern for: (a) graphite-based samples and (b) graphene-based samples.

This reflection confirms the well-ordered layered structure associated with stacked graphene sheets. Additionally, a low-intensity secondary phase (♦) was detected in GW. The crystalline phase was identified using the ICDD Powder Diffraction File (PDF-2) database. The diffraction pattern matched orthorhombic zinc sulphate heptahydrate ($ZnSO_4 \cdot 7H_2O$), card no. 01-075-0949.

The presence of zinc sulfate in spent AA batteries, particularly in the graphite rod region, is associated with corrosion and oxidation of the metallic zinc casing (anode) during discharge. Under operating conditions, zinc reacts with internal battery components, including the electrolyte, leading to the formation of zinc-containing compounds such as zinc chloride or zinc sulfate, which may subsequently migrate through the graphite rod and the manganese dioxide paste.

Importantly, although hydrated zinc sulfate was detected as a minor contaminant in GW, its presence did not affect the structural evolution of graphene oxide (GOW) or reduced graphene oxide (rGOW). Raman and solid-state NMR confirmed that the characteristic structural features of GO and rGO

(defect-related bands, graphitic domain organization, and oxygen-functionalized carbon environments) were fully preserved after oxidation and thermal reduction. These findings demonstrate that residual zinc sulfate does not interfere with either the oxidation kinetics or the subsequent reduction process, so that no additional pre-treatment with strong acids or organic solvents is required to eliminate this impurity; an outcome fully aligned with the principles of green chemistry and process simplification.

Figure 5b shows broad diffraction peaks characteristic of graphene-based materials, namely GOW (2θ = 10.5°), rGOW (2θ = 25.1°), and GOC (2θ = 7.7°). The emergence of these reflections, particularly the low-angle peaks observed for GOW and GOC, is associated with exfoliation of the graphite layers and incorporation of oxygen-containing functional groups, which increase the interlayer spacing relative to pristine graphite (Gebreegziabher, 2019; Mokoena, 2024; Bu, 2023; Hosseinkhani, 2023).

According to Bragg's law, the corresponding interlayer spacings ($d_{002}$) were calculated to be 0.842 nm for GOW (2θ = 10.5°), 0.355 nm for rGOW (2θ = 25.1°), and 1.15 nm for GOC (2θ = 7.7°), confirming the significant lattice expansion induced by oxidation (Table 1).

Upon thermal reduction, the partial removal of oxygenated functional groups and intercalated water molecules promotes a marked decrease in interlayer distance, resulting in the reappearance of a diffraction peak at 2θ = 25.1° in the XRD pattern of rGOW (d ≈ 0.355 nm), close to the characteristic spacing of crystalline graphite (0.338 nm).

However, this peak remains broader than that of the parent graphite (Fig. 5a) — and even broader than the (002) reflection of GOW itself, as reflected in its larger FWHM (β = 0.0356 rad for rGOW vs. 0.0245 rad for GOW; Table 1). This indicates that the thermal treatment at 150 °C was sufficient to largely collapse the oxygen-expanded interlayer gallery, but insufficient to restore long-range stacking coherence along the c-axis: the crystallite size of rGOW (Lc = 3.85 nm) is in fact smaller than that of GOW (Lc = 5.60 nm), despite its d(002) being much closer to the graphitic value (Vieira, 2023).

Table 1 summarizes the crystallographic parameters of the investigated samples, including the interplanar spacing (d) and the average crystallite size (Lc), calculated according to Equations 1 and 2.

**Table 1.** XRD and Raman parameters

| XRD | | | | | | | | |
|---|---|---|---|---|---|---|---|---|
| **Sample** | **2θ (º)** | **θ (º)** | **2θ (rad)** | **θ (rad)** | **$d_{(002)}$ (nm)** | **β (rad)** | **$L_c$ (nm)** | **$G_{(\%)}$** |
| GW | 26.4 | 13.2 | 0.461 | 0.2305 | 0.338 | $4.189 \cdot 10^{-3}$ | 32.8 | 69.7 |
| CG | 26.4 | 13.2 | 0.461 | 0.2305 | 0.338 | $4.189 \cdot 10^{-3}$ | 32.8 | 69.7 |
| GOW | 10.5 | 5.25 | 0.183 | 0.0915 | 0.842 | 0.0245 | 5.60 | N/A |
| rGOW | 25.1 | 12.55 | 0.438 | 0.219 | 0.355 | 0.0356 | 3.85 | N/A |
| GOC | 7.7 | 3.85 | 0.134 | 0.067 | 1.15 | 0.0359 | 3.82 | N/A |
| **Raman** | | | | | | | | |
| **Sample** | **$I_D$ ($cm^{-1}$)** | **$I_G$ ($cm^{-1}$)** | **$I_{2D}$ ($cm^{-1}$)** | **$I_D/I_G$** | **$I_{2D}/I_G$** | **$L_a$ (nm)** | | |
| GW | 1328.3 | 1560.0 | 2670.3 | 0.85 | 1.712 | 22.6 | | |
| CG | 1340.6 | 1561.6 | 2696.9 | 0.86 | 1.727 | 22.3 | | |
| GOW | 1330.3 | 1560.1 | 2661.1 | 0.85 | 1.706 | 22.6 | | |
| rGOW | 1339.8 | 1572.5 | 2661.1 | 0.85 | 1.692 | 22.6 | | |
| GOC | 1339.8 | 1579.1 | 2673.5 | 0.85 | 1.693 | 22.6 | | |

The graphite samples GW and CG exhibited identical values (d = 0.338 nm, Lc = 32.8 nm), confirming that GW possesses crystallographic quality comparable to that of high-purity commercial graphite (CG). The degree of graphitization (Eq. 3) was also essentially identical for both precursors (G = 69.7%), despite the presence of minor impurities in GW, demonstrating that graphite recovered from e-waste preserves its structural integrity even after complete battery discharge.

Considering the well-established correlation between the crystallographic quality of the precursor and that of the derived graphene oxide, GOW exhibited a larger stacking crystallite size (Lc = 5.60 nm) than commercial GOC (Lc = 3.82 nm), pointing to a somewhat less complete exfoliation of GOW rather than a difference in the intrinsic quality of the two precursors. As shown in Table 1, the interplanar spacing of GOW (d = 0.842 nm) is also notably smaller than that of GOC (d = 1.15 nm), indicating a lower oxidation degree in GOW.

One of the most influential factors affecting the efficiency of the oxidation process is the particle size of the graphite precursor (Vieira, 2016). SEM micrographs suggest that CG consists of smaller and more dispersed particles, whereas GW tends to form larger aggregates. The smaller particle size of CG

likely facilitated more effective intercalation and oxidation, leading to a higher oxidation degree in GOC and, consequently, a greater expansion of the interlayer spacing.

Nevertheless, despite its slightly lower oxidation degree, GOW exhibits structural characteristics fully consistent with those expected for graphene oxide, demonstrating that graphite recovered from spent batteries remains a suitable and reliable precursor for the production of high-quality graphene-based materials.

A further decrease in interlayer spacing was observed for rGOW (d = 0.355 nm) as a result of the thermal reduction of GOW, which removes oxygen-containing functional groups and partially restores interlayer interactions between graphene sheets (Gebreegziabher, 2019; Mokoena, 2024; Vieira, 2016; Bu, 2023; Hosseinkhani, 2023).

However, as noted above, this contraction in d(002) is not accompanied by a recovery of Lc: the crystallite size of rGOW (3.85 nm) is smaller than that of GOW (5.60 nm) and comparable to that of GOC (3.82 nm), indicating that

gallery collapse upon thermal reduction is not equivalent to restoration of long-range graphitic order.

The crystallographic parameters obtained from XRD confirm that graphite recovered from spent batteries (GW) exhibits structural characteristics virtually identical to those of commercial graphite (CG), including interplanar spacing (d(002) = 0.338 nm), crystallite size (Lc = 32.8 nm), and degree of graphitization (69.7%).

These results demonstrate that the graphite rod in Zn–C batteries retains a high degree of crystallinity even after complete electrochemical discharge, since it primarily functions as a current collector during operation. Consequently, GW represents a high-quality carbon precursor for graphene oxide synthesis, comparable to high-purity commercial graphite.

### 3.3 Raman

Figure 6 shows the Raman spectra recorded for (a) GW and CG, and (b) GOW, rGOW, and GOC. All samples exhibited the characteristic D, G, and 2D bands typically associated with graphitic- and graphene-based materials, in agreement

with previous reports (Gebreegziabher, 2019; Mokoena, 2024; Raman, 1928; Bu, 2023; Hosseinkhani, 2023; Tuinstra, 1970).

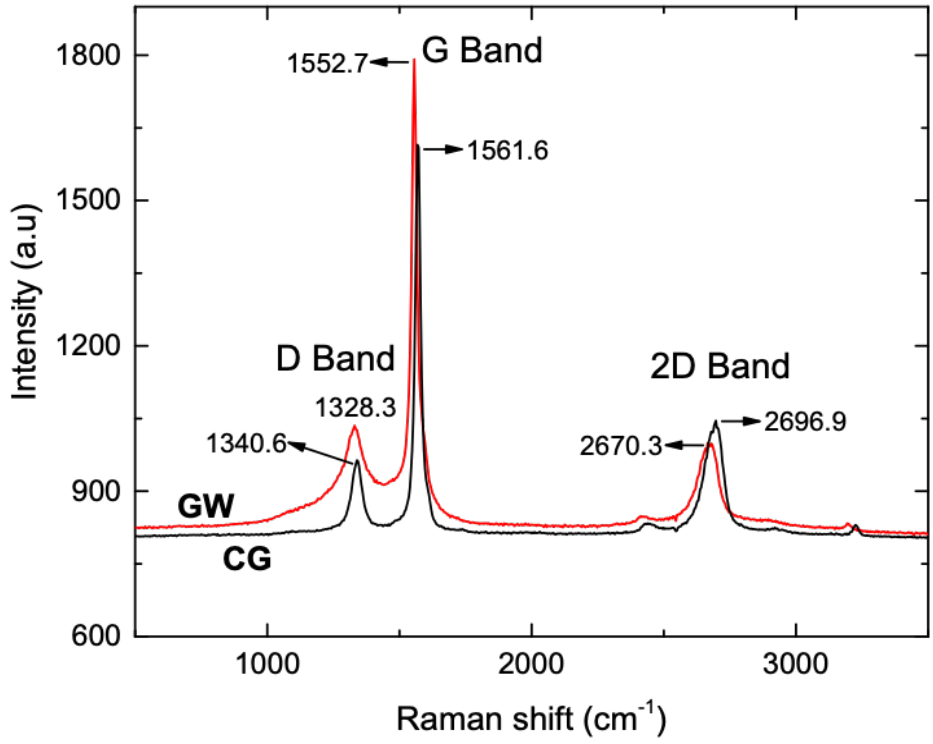


(a)

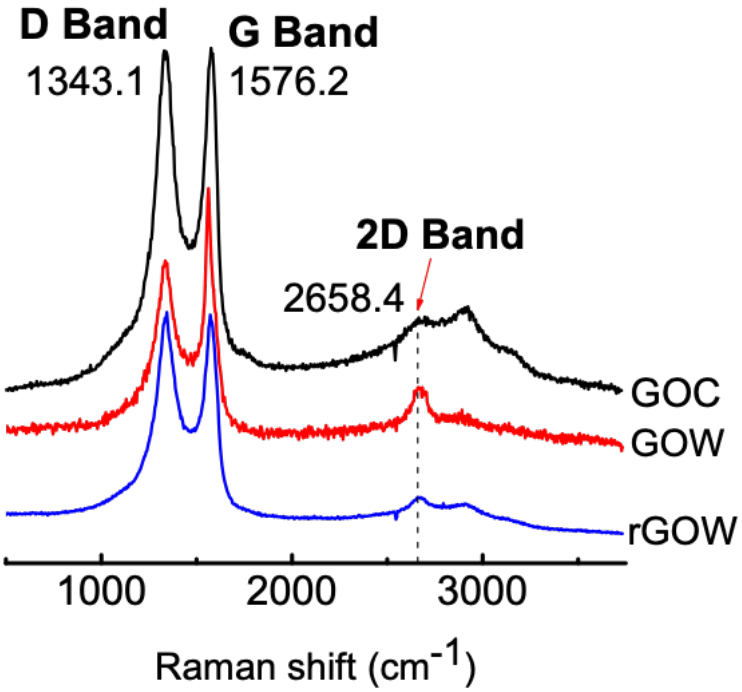


(b)

**Figure 6.** Raman spectra obtained for: (a) graphite-based samples and (b) graphene-based samples.

The Raman G band, observed between 1560 and 1579 $cm^{-1}$, corresponds to the in-plane vibration of $sp^2$-hybridized carbon atoms, whereas the D band, located between 1328 and 1341 $cm^{-1}$, arises from the breathing modes of $sp^2$ carbon rings activated by structural defects and lattice disorder (Okhai, 2016).

The graphite samples GW and CG exhibited similar $I_D/I_G$ ratios (0.85 and 0.86, respectively), indicating comparable defect densities and confirming that the graphite recovered from spent batteries retains a structural quality equivalent to that of high-purity commercial graphite. According to the Tuinstra–Koenig relation, the $I_D/I_G$ ratio is inversely proportional to the in-plane crystallite size (La) of $sp^2$ domains, so comparable $I_D/I_G$ values indicate similar average domain sizes in both graphite precursors.

Notably, the $I_D/I_G$ ratio of GOW, rGOW, and GOC (0.85 in all three samples; Table 1) remained essentially unchanged relative to the graphite precursors (0.85–0.86), rather than increasing as might be expected from the introduction of oxygen-containing functional groups. Using the Cançado relation (Eq. 4), the corresponding $L_a$ values are correspondingly stable across the whole sample series (22.3–22.6 nm; Table 1), showing that the lateral extension of the $sp^2$ conjugated domains was preserved throughout the oxidation–reduction pathway.

This behavior indicates that the structural disorder introduced by oxidation predominantly disrupts the interlayer stacking order along the c-axis, as clearly evidenced by the large increase in d(002) and the pronounced decrease in Lc

reported by XRD (Section 3.2), rather than fragmenting the in-plane graphitic domains that Raman spectroscopy probes through $I_D/I_G$ and La.

The introduction of oxygen-containing functional groups during oxidation is expected to generate localized $sp^3$-hybridized carbon centres and additional edge or defect sites. However, this chemical modification is not reflected in a measurable increase of the $I_D/I_G$ ratio relative to the graphite precursors, which already display a comparatively high D-band contribution ($I_D/I_G$ = 0.85–0.86).

This suggests that the point-defect density probed by the Raman D band was already substantial in the precursor graphite, likely associated with finite crystallite size and abundant edge/grain-boundary defects inherent to both the waste-derived and commercial starting materials, such that the additional defects introduced by oxidation did not produce a further detectable increase in $I_D/I_G$.

A slight redshift of the D and 2D bands is observed for GOW (1330.3 and 2661.1 $cm^{-1}$) relative to GOC (1339.8 and 2673.5 $cm^{-1}$), consistent with a lower degree of oxygenation and local lattice distortion in GOW, in agreement with its

smaller interlayer expansion measured by XRD (d = 0.842 nm for GOW vs. 1.15 nm for GOC).

This trend is corroborated by the position of the G band, which shifts only marginally for GOW (1560.1 $cm^{-1}$, essentially unchanged from graphite) but is clearly blue-shifted for GOC (1579.1 $cm^{-1}$) relative to CG (1561.6 $cm^{-1}$), consistent with a higher oxidation degree in GOC, as independently indicated by XRD. The I2D/IG ratio of GOW (1.706) closely matches that of GOC (1.693), indicating that graphene oxide obtained from recovered battery graphite preserves a layer-stacking organisation comparable to that produced from high-purity commercial graphite.

After thermal reduction, rGOW retained an ID/IG ratio (0.85) identical to that of GOW, indicating that no additional in-plane defects were generated, nor were pre-existing point defects annealed, during the 150 °C treatment, as detected by Raman spectroscopy. In contrast, XRD showed that the interlayer spacing of rGOW contracted markedly toward the graphitic value (d = 0.355 nm), while its crystallite size along the c-axis decreased further relative to GOW ($L_c$ = 3.85 nm vs. 5.60 nm).

Taken together, these results show that thermal treatment promotes gallery collapse (interlayer contraction) without producing well-ordered, coherently stacked graphitic domains, and without measurably altering the in-plane $sp^2$ network, a behavior typical of reduced graphene oxide, in which graphitic ordering along the c-axis is recovered only partially and heterogeneously, while in-plane defects generated during oxidation are not readily healed by mild thermal treatment.

Overall, the Raman results confirm that graphite recovered from spent batteries serves as an effective carbon precursor for graphene oxide synthesis, producing a GOW material with spectroscopic characteristics ($I_D/I_G$, $I_{2D}/I_G$, and $L_a$) essentially indistinguishable from those obtained from commercial graphite (GOC).

The complementary XRD analysis ($L_c$, d(002)) shows that the two techniques probe different structural dimensions, $L_a$ reflects the lateral extension of ordered $sp^2$ domains within individual graphene sheets, whereas L represents the vertical stacking order of graphene layers, and, taken together, indicate that the oxidation–reduction pathway investigated here reorganizes the interlayer (c-axis) structure far more than the in-plane graphitic framework. The intensity

values of the D, G, and 2D bands, together with the corresponding $I_D/I_G$ and $I_{2D}/I_G$ ratios and La values, are summarized in Table 1 (Cançado, 2006).

### 3.4 NMR

Figure 7 displays the solid-state $^{13}C$ NMR spectra of the graphene-based samples. All spectra exhibit a broad resonance characteristic of $sp^2$-hybridized carbon atoms (C=C), centred at 127.9 ppm for GOW, 133.7 ppm for GOC, and 126.1 ppm for rGOW (Vieira, 2016; Costa, 2023).

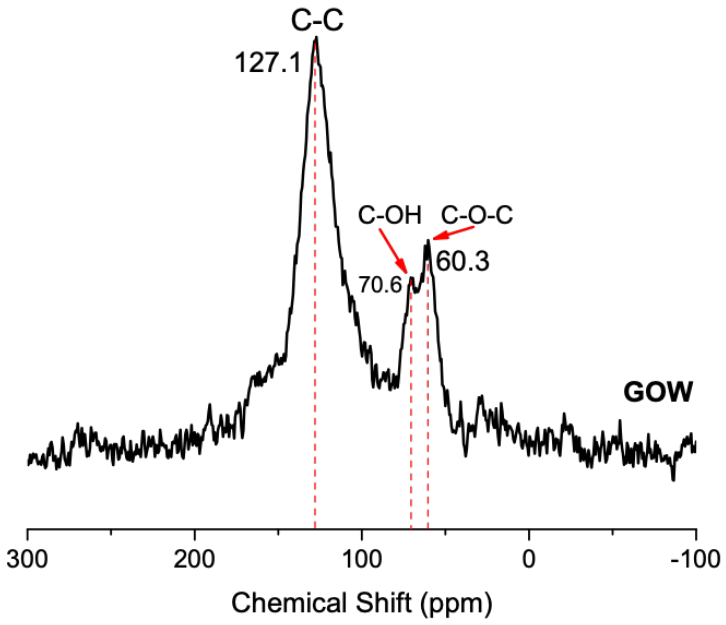


(a)

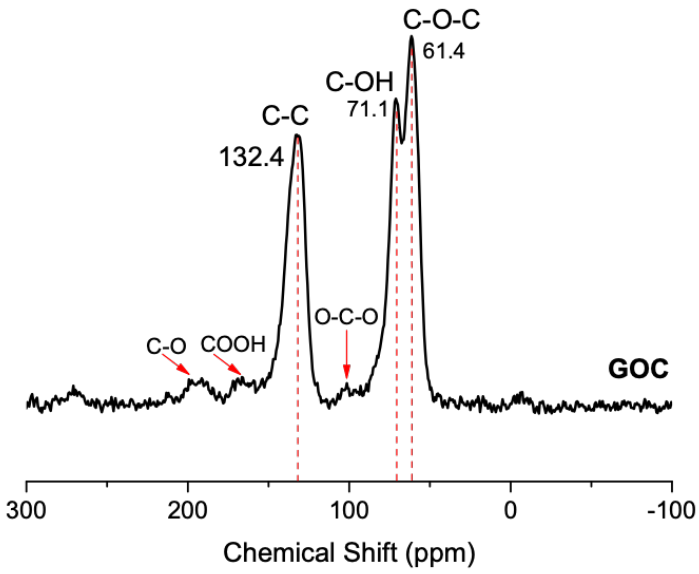


(b)

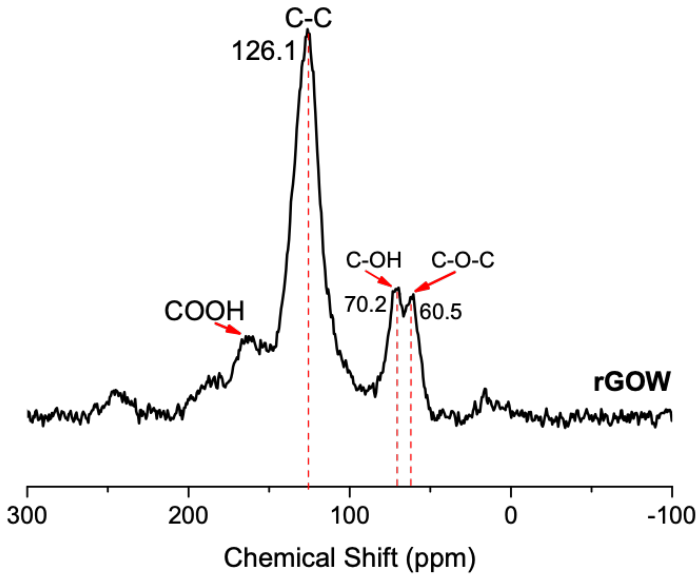


(c)

**Figure 7.** NMR spectra recorded for the analyzed samples: (a) GOW, (b) GOC, and (c) rGOW.

This chemical-shift variation among GOC, GOW, and rGOW reflects differences in the local electronic environment of the $sp^2$-hybridized carbons, consistent with the oxidation degree of each sample. Rather than reflecting a change in the lateral size of the $sp^2$ domains, which Raman spectroscopy (Section 3.3) indicates remains essentially constant ($L_a \approx 22–23$ nm) across GOW, rGOW, and GOC, this trend is more consistent with differences in the density and proximity of oxygen-containing functional groups directly bonded to, or adjacent to, the aromatic $sp^2$ network.

GOC, identified by XRD as the most heavily oxidised sample (d(002) = 1.15 nm; Section 3.2), shows the largest downfield shift (133.7 ppm), consistent with a higher density of electron-withdrawing oxygen functionalities perturbing the local magnetic shielding at the $^{13}C$ nuclei. GOW, which XRD indicates is less extensively oxidised (d(002) = 0.842 nm), shows a smaller shift (127.9 ppm), closer to the $sp^2$ carbon environment of pristine graphite.

The resonances due to carbons bonded to different types of oxygen-containing functional groups (such as hydroxyls, epoxides, and carboxylic acids) are observed in the 60–80 ppm (region A) and 160–180 ppm (region B) ranges in

the spectra obtained for GOC and GOW samples (Fig. 7) (Vieira, 2016; Costa, 2023).

In contrast, the rGOW spectrum exhibits a marked reduction in these signals, indicating effective deoxygenation and partial restoration of the $sp^2$-conjugated carbon network (Vieira, 2016), consistent with the pronounced interlayer contraction observed by XRD (d = 0.355 nm, approaching the graphitic value of 0.338 nm; Section 3.2). The $sp^2$ carbon resonance shifts further upfield in rGOW (126.1 ppm) relative to GOW (127.9 ppm), approaching a more graphite-like electronic environment.

However, as with the XRD- and Raman-derived parameters (Sections 3.2–3.3), this recovery remains only partial: the 126.1 ppm value does not fully coincide with that of pristine graphite, mirroring the incomplete restoration of long-range stacking order (Lc = 3.85 nm for rGOW vs. 32.8 nm for graphite) and the unchanged $I_D/I_G$ ratio observed by Raman.

These findings validate the successful conversion of GOW into rGOW, consistent with the expected structural and electronic recovery, while confirming

across all three techniques, that the reduction achieved under the mild thermal conditions used here (150 °C, 15 h) is partial rather than complete.

**Conclusion**

Graphite rods from spent Zn–C AA batteries were converted directly into graphene oxide (GOW) by a modified Hummers method after only water washing, drying and sieving, with no acid leaching or solvent-based purification.

Despite residual $ZnSO_4 \cdot 7H_2O$, GOW displayed the structural signature of graphene oxide, with Raman features ($I_D/I_G \approx 0.85$; $L_a \approx 22.6$ nm) comparable to those of GO from commercial graphite prepared under identical conditions (GOC). Its oxidation degree was somewhat lower (d = 0.842 vs 1.15 nm), which we attribute to the coarser recovered particles.

A single thermal treatment (150 °C, 15 h) without chemical reductants collapsed the interlayer spacing to 0.355 nm, markedly attenuated the oxygenated-carbon signals and shifted the $sp^2$ resonance from 127.9 to 126.1 ppm. The reduction is partial ($L_c$ = 3.85 nm), but it avoids hazardous reductants and their associated waste.

Combining direct oxidation of minimally treated waste graphite with reductant-free thermal reduction, benchmarked against commercial graphite, shows that spent Zn–C battery graphite is a technically viable secondary precursor for graphene-based materials.

These results establish spent Zn–C battery graphite as a technically viable secondary precursor that turns an overlooked municipal solid waste fraction into a raw material for graphene-based materials, keeping carbon in productive use in line with circular economy principles.

**Acknowledgements - Funding**

The authors would like to thank CAPES (Coordination for the Improvement of Higher Education Personnel - Brazilian Federal Agency, Financing Code 001) for financial support. This work was carried out with the support of the Fundação de Amparo à Pesquisa e Inovação do Espírito Santo (FAPES) - T.O. 2025-4DF3V. Our thanks to the Laboratories LabMinst (Multiuser Instrumentation Laboratory – LabPetro, UFES, Brazil) for performing NMR and Raman measurements, and to LUCCAR (Carlos Alberto Redins Laboratory of Cellular Ultrastructure) for performing SEM images.

## Declaration of Competing Interests

The authors declare that they have no known competing financial interests or personal relationships that could have appeared to influence the work reported in this paper.

## Author Contributions

Brito, G. M.: Conceptualization, Methodology, Writing and Editing - Original draft preparation, Data curation.

Santos, G. M.: Reviewing and Editing.

Cipriano, D. F.: Reviewing and Editing,

Schettino Jr., M. A.: Reviewing and Editing.

Freitas, J. C. C.: Supervision, Reviewing.

## Data Availability

The datasets generated during and/or analyzed during the current study are not publicly available due to intellectual property considerations related to ongoing technology development but are available from the corresponding author on reasonable request.

## References

Adu, J. T., Aneke, F. I. (2025) Evaluation of heavy metal contamination in landfills from e-waste disposal and its potential as a pollution source for surface water bodies. Results in Engineering 25, 104431. https://doi.org/10.1016/j.rineng.2025.104431

Ahmed, A., Singh, A., Young, S. J., Gupta, V., Singh, M., Arya, S. (2023) Synthesis techniques and advances in sensing applications of reduced graphene oxide composites: A review. Composites Part A 165, 107373. https://doi.org/10.1016/j.compositesa.2022.107373

Bokobza, L., Bruneel, J.-L., Couzi, M. (2015) Raman spectra of carbon-based materials (from graphite to carbon black) and of some silicone composites. C 1, 77-94. https://doi.org/10.3390/c1010077

Bu, Y., Kim, B. S. (2023) Eco-friendly production of functionalized few-layer graphene using coffee waste extract and in-situ growth of copper oxide nanoparticles. Journal of Environmental Chemical Engineering 11, 109350. https://doi.org/10.1016/j.jece.2023.109350

Cançado, L. G., Takai, T., Enoki, T. (2006) General equation for determination of the crystallite size La of nanographite by Raman spectroscopy. Applied Physics Letters 88, 163106. https://doi.org/10.1063/1.2196057

Chakraborty, S. C., Qamruzzaman, M., Zaman, M. W. U., Alam, M. M., Hossain, M. D., Pramanik, B. K., Nguyen, L. N., Nghiem, L. D., Ahmed, M. F., Zhou, J. L.,

Mondal, M. I. H. (2022) Metals in e-waste: Occurrence, fate, impacts and remediation technologies. Process Safety and Environmental Protection 162, 230-252. https://doi.org/10.1016/j.psep.2022.04.011

Costa, T. L. G., Vieira, M. A., Gonçalves, G. R., Cipriano, D. F., Valdemar, L. Jr., Gonçalves, A. S., Scopel, W. L., De Siervo, A., Freitas, J. C. C. (2023) Combined computational and experimental study about the incorporation of phosphorus into the structure of graphene oxide. Physical Chemistry Chemical Physics 25, 6927-6943. https://doi.org/10.1039/D2CP03666E

Cullity, B. D., Stock, S. R. (2001) Elements of X-ray Diffraction, 3rd ed., Prentice Hall.

D'Amato, D., Droste, N., Allen, B., Kettunen, M., Lahtinen, K., Korhonen, J., Leskinen, P., Matthies, B. D., Toppinen, A. (2017) Green, circular, bio economy: A comparative analysis of sustainability avenues. Journal of Cleaner Production 168, 716-734. https://doi.org/10.1016/j.jclepro.2017.09.053

Destiarti, L., Huda, B. N., Riyanto, R., Roto, R., Mudasir, M. (2024) Challenges of using natural extracts as green reducing agents in the synthesis of rGO: A brief review. Results in Chemistry 7, 101270. https://doi.org/10.1016/j.rechem.2023.101270

Dreyer, D. R., Park, S., Bielawski, C. W., Ruoff, R. S. (2010) The chemistry of graphene oxide. Chemical Society Reviews 39, 228–240. https://doi.org/10.1039/b917103g

Fernández-Merino, M. J., Guardia, Paredes, J. I., Villar-Rodil, S., Solís-Fernández, P., Martínez-Alonso, A., Tascón, J. M. D. (2010) Vitamin C is an ideal substitute for hydrazine in the reduction of graphene oxide suspensions. Journal of Physical Chemistry C 114, 6426-6432. https://doi.org/10.1021/jp100603h

Freitas, J. C. C., Cunha, A. G., Emmerich, F. G. (2012) Solid-state nuclear magnetic resonance methods applied to the study of carbon materials. In: Chemistry and Physics of Carbon, Vol. 31, CRC Press.

Gao, W., Alemany, L. B., Ci, L., Ajayan, P. M. (2009) New insights into the structure and reduction of graphite oxide. Nature Chemistry 1, 403-408. https://doi.org/10.1038/nchem.281

Gebreegziabher, G. G., Asemahegne, A. S., Ayele, D. W., Dhakshnamoorthy, M. (2019) One-Step synthesis and characterization of reduced graphene oxide using chemical exfoliation method. Materials Today Chemistry 12, 233-239. https://doi.org/10.1016/j.mtchem.2019.02.003

Geim, A. K., Novoselov, K. S. (2007) The rise of graphene. Nature Materials 6, 183-191.

He, H., Riedl, T., Lerf, A., Klinowski, J. (1996) Solid-state NMR studies of the structure of graphite oxide. Journal of Physical Chemistry 100, 19954-19958.

Hosseinkhani, O., Hamzehlouy, A., Dan, S., Sanchouli, N., Tavakkoli, M., Hashemipour, H. (2023) Graphene oxide/ZnO nanocomposites for efficient

removal of heavy metal and organic contaminants from water. Arabian Journal of Chemistry 16, 105176. https://doi.org/10.1016/j.arabjc.2023.105176

Houessionon, M. K., Ouendo, E. M. D., Bouland, C., Takyi, S. A., Kedote, N. M., Fayomi, B., Fobil, J. N., Basu, N. (2021) Environmental heavy metal contamination from electronic waste (e-waste) recycling activities worldwide: A systematic review from 2005 to 2017. International Journal of Environmental Research and Public Health 18, 3517. https://doi.org/10.3390/ijerph18073517

Hummers Jr, W. S., Offeman, R. E. (1958) Preparation of Graphitic Oxide. Journal of the American Chemical Society 80, 1339. http://dx.doi.org/10.1021/ja01539a017

Ida, T. K., Sonowal, K., Golder, A. K., Mandal, B. (2025) Simple environmental-friendly method for graphite recovery from spent lithium-ion batteries and its utilization for the synthesis of graphene oxide. Separation and Purification Technology 374, 133758. https://doi.org/10.1016/j.seppur.2025.133758

Iwashita, N., Park, C. R., Fujimoto, H., Shiraishi, M., Inagaki, M. (2004) Specification for a standard procedure of X-ray diffraction measurements on carbon materials. Carbon 42, 701-714. https://doi.org/10.1016/j.carbon.2004.02.008

Jirickova, A., Jankovsky, O., Sofer, Z., Sedmidubsky, D. (2022) Synthesis and applications of graphene oxide. Materials 15, 1-21. https://doi.org/10.3390/ma15030920

Kondratowicz, I., Nadolska, M., Zelechowska, K. (2018) Reduced graphene oxide to teach undergraduate students core chemistry and nanotechnology concepts. Journal of Chemical Education 95, 1012-1017. https://doi.org/10.1021/acs.jchemed.7b00568

Lee, Y. S., Ji, B. C., Seo, J. W., Jeong, D. I., Kwon, S. B., Yoo, J. H., Kang, B. G., Song, Y. H., Yang, W. S., Kang, B. K., Yoon, D. H. (2023) Facile recyclable process of high-quality single layer graphene oxide via waste graphite anode scrap. Ceramics International 49, 34774-34779. https://doi.org/10.1016/j.ceramint.2023.08.149

Lerf, A., He, H., Forster, M., Klinowski, J. (1998) Structure of graphite oxide revisited. Journal of Physical Chemistry B 102, 4477-4482. https://doi.org/10.1021/jp9731821

Luo, D., Zhang, G., Liu, J., Sun, X. (2011) Evaluation criteria for reduced graphene oxide. Journal of Physical Chemistry C 115, 11327-11335. https://doi.org/10.1021/jp110001y

Marcano, D. C., Kosynkin, D. V., Berlin, J. M., Sinitskii, A., Sun, Z., Slesarev, A., Alemany, L. B., Lu, W., Tour, J. M. (2010) Improved synthesis of graphene oxide. ACS Nano 4, 4806–4814. https://doi.org/10.1021/nn1006368

Mishra, R., Kumar, A., Singh, E., Kumari, A., Kumar, S. (2023) Synthesis off graphene oxide from biomass waste: Characterization and volatile compounds removal. Process Safety and Environmental Protection 180, 800-807. https://doi.org/10.1016/j.psep.2023.10.048

Mokoena, L. S., Mofokeng, J. P. (2024) Synthesis and characterization of graphene oxide (GO) for the removal of lead ions in water. Carbon Trends 15, 100339. https://doi.org/10.1016/j.cartre.2024.100339

Mulligan-Clarke, B., Davids, C., Mushtaq, M., Moraes Leite, M., Geaney, H., Kellici, S., Kennedy, T. (2026) Sustainable synthesis of a high-performing off-stoichiometric sodium iron sulfate/N-rGO composite cathode for sodium-ion batteries. Journal of Power Sources 668, 239320. https://doi.org/10.1016/j.jpowsour.2026.239320

Mushahary, N., Sarkar, A., Basumatary, F., Brahma, S., Das, B., Basumatary, S. (2024) Recent developments on graphene oxide and its composite materials: From photocatalysis, supercapacitors, sensors and antimicrobial activity. Results in Surfaces and Interfaces 15, 100225. https://doi.org/10.1016/j.rsurfi.2024.100225

Okhai, O., Gonçalves, G., Tkach, A., Dias, C., Ventura, J., Silva, M. F. R., Gonçalves, L. M. V., Titus, E. (2016) Thin film versus paper-like reduced graphene oxide: Comparative study of structural, electrical, and thermoelectrical properties. Journal of Applied Physics 120, 051706.

Raman, C. V., Krishnan, K. S. (1928) A new type of secondary radiation. Nature 121, 501-502.

Rawal, A., Man, S. H. C., Agarwal, V., Yao, Y., Thickett, S. C., Zetterlund, P. B. (2021) Structural complexity of graphene oxide: The Kirigami model. ACS

Applied Materials & Interfaces 13, 18255-18263. https://doi.org/10.1021/acsami.1c01157

Rezaei, M., Nekahi, A., Kumar, A. M. R., Nizami, A., Li, X., Deng, S., Nanda, J., Zaghib, K. (2025) A review of lithium-ion battery recycling for enabling a circular economy. Journal of Power Sources 630, 236157. https://doi.org/10.1016/j.jpowsour.2024.236157

Ribeiro, J. S., Freitas, M. B. J. G., Freitas, J. C. C. (2021) Recycling of graphite and metals from spent Li-ion batteries aiming the production of graphene/CoO-based electrochemical sensors. Journal of Environmental Chemical Engineering 9, 104689. https://doi.org/10.1016/j.jece.2020.104689

Saha, O., Kabir, M. D., Islam, M. M., Bashar, M. S., Pabel, M. Y., Yasmin, S. (2025) Recycling spent dry cells into rGO/$MnO_2$ nanocomposites for advanced supercapacitor electrodes. RSC Advances 15, 41874-41885. https://doi.org/10.1039/D5RA04072H

Singh, S. B., Haskin, N., Dastgheib, S. A. (2023) Coal-based graphene oxide-like materials: A comprehensive review. Carbon 215, 118447. https://doi.org/10.1016/j.carbon.2023.118447

Soni, M., Kumar, P., Pandey, J., Sharma, S. K., Soni, A. (2018) Scalable and site specific functionalization of reduced graphene oxide for circuit elements and flexible electronics. Carbon 128, 172-178. https://doi.org/10.1016/j.carbon.2017.11.087

Stobinski, L., Lesiak, B., Malolepszy, A., Mazurkiewicz, M., Mierzwa, B., Zemek, J., Jiricek, P., Bieloshapka, I. (2014) Graphene oxide and reduced graphene oxide studied by the XRD, TEM and electron spectroscopy methods. Journal of Electron Spectroscopy and Related Phenomena 195. https://doi.org/10.1016/j.elspec.2014.07.003

Tuinstra, F., Koenig, J. L. (1970) Raman spectrum of graphite. Journal of Chemical Physics 53, 1126-1130. https://doi.org/10.1063/1.1674108

Uppin, B., Sankannavar, R., Kangutkar, R., Jayappa, M., Kolekar, S., Nayaka, G. P. (2025) Recovery of intercalated Li and synthesis of reduced graphene oxide from graphite of spent Li-ion battery for supercapacitor application. Inorganic Chemistry Communications 177, 114371. https://doi.org/10.1016/j.inoche.2025.114371

Vieira, M. A., Gonçalves, G. R., Cipriano, D. F., Schettino Jr, M. A., Filho, E. A. S., Cunha, A. G., Emmerich, F. G., Freitas, J. C. C. (2016) Synthesis of graphite oxide from milled graphite studied by solid-state 13C nuclear magnetic resonance. Carbon 98, 496-503. https://doi.org/10.1016/j.carbon.2015.11.037

Vieira, M. A., Costa, T. L. G., Gonçalves, G. R., Cipriano, D. F., Schettino, M. A., Silva, E. L., Cuna, A., Freitas, J. C. C. (2023) Phosphorus/sulfur-enriched reduced graphene oxide papers obtained from recycled graphite: Solid-state NMR characterization and electrochemical performance for energy storage. Journal of Carbon Research 9, 60. https://doi.org/10.3390/c9020060

Wu, Z., Ren, W., Gao, L., Liu, B., Jiang, C., Cheng, H. (2009) Synthesis high quality graphene with a pre-determined number of layers. Carbon 47, 493-499. https://doi.org/10.1016/j.carbon.2008.10.031

Yoon, D., Cheong, H. (2012) Raman spectroscopy for characterization of graphene. In: Raman Spectroscopy for Nanomaterials Characterization. Springer. https://doi.org/10.1007/978-3-642-20620-7_9

Zheng, L., Zhang, G., Zhang, M., Guo, S., Liu, Z. (2012) Preparation and capacitance performance of Ag-graphene based nanocomposite. Journal of Power Sources 201, 376-381. https://doi.org/10.1016/j.jpowsour.2011.11.026

Zhou, Z., Bouwman, W. G., Schut, H., Pappas, C. (2014) Interpretation of X-ray diffraction patterns of (nuclear) graphite. Carbon 69, 17-24. https://doi.org/10.1016/j.carbon.2013.11.032

Zhu, H., Li, W., Sun, L. (2024) Application of graphite-derived materials in metal-ion batteries. Journal of Energy Storage 102, 114095. https://doi.org/10.1016/j.est.2024.114095